

Article

Relationship between Apparent Diffusion Coefficient Distribution and Cancer Grade in Prostate Cancer and Benign Prostatic Hyperplasia

Shigeyoshi Saito ^{1,2,*} , Yoshihiro Koyama ³, Junpei Ueda ¹ and Takashi Hashido ³

¹ Department of Medical Physics and Engineering, Division of Health Sciences, Osaka University Graduate School of Medicine, Osaka 565-0871, Japan; uedaj@sahs.med.osaka-u.ac.jp

² Department of Advanced Medical Technologies, National Cerebral and Cardiovascular Center Research Institute, Osaka 565-0871, Japan

³ Department of Medical Technology, Division of Radiology, Osaka University Hospital, Osaka 564-8565, Japan; koyamayo@hp-rad.med.osaka-u.ac.jp (Y.K.); t_hashido@hp-rad.med.osaka-u.ac.jp (T.H.)

* Correspondence: saito@sahs.med.osaka-u.ac.jp; Tel.: +81-6-6879-2619

Abstract: The aim of this paper was to assess the associations between prostate cancer aggressiveness and histogram-derived apparent diffusion coefficient (ADC) parameters and determine which ADC parameters may help distinguish among stromal hyperplasia (SH), glandular hyperplasia (GH), and low-grade, intermediate-grade, and high-grade prostate cancers. The mean, median, minimum, maximum, and 10th and 25th percentile ADC values were determined from the ADC histogram and compared among two benign prostate hyperplasia (BPH) groups and three Gleason score (GS) groups. Seventy lesions were identified in 58 patients who had undergone prostatectomy. Thirty-nine lesions were prostate cancers (GS 6 = 7 lesions, GS 7 = 19 lesions, GS 8 = 11 lesions, GS 9 = 2 lesions), and thirty-one lesions were BPH (SH = 15 lesions, GH = 16 lesions). There were statistically significant differences in 10th percentile and 25th percentile ADC values when comparing GS 6 to GS 7 ($p < 0.05$). The 10th percentile ADC values yielded the highest area under the curve (AUC). Tenth and 25th percentile ADCs can be used to more accurately differentiate lesions with GS 6 from those with GS 7 than other ADC parameters. Our data indicate that the major challenge with ADC mapping is to differentiate between SH and GS 6, and SH and GS 7.

Keywords: histogram-derived ADC parameters; stromal hyperplasia; glandular hyperplasia; prostate cancer; benign prostate hyperplasia



Citation: Saito, S.; Koyama, Y.; Ueda, J.; Hashido, T. Relationship between Apparent Diffusion Coefficient Distribution and Cancer Grade in Prostate Cancer and Benign Prostatic Hyperplasia. *Diagnostics* **2022**, *12*, 525. <https://doi.org/10.3390/diagnostics12020525>

Academic Editors: Cecilia Di Ruberto, Alessandro Stefano, Albert Comelli, Lorenzo Putzu and Andrea Loddo

Received: 2 January 2022

Accepted: 17 February 2022

Published: 18 February 2022

Publisher's Note: MDPI stays neutral with regard to jurisdictional claims in published maps and institutional affiliations.



Copyright: © 2022 by the authors. Licensee MDPI, Basel, Switzerland. This article is an open access article distributed under the terms and conditions of the Creative Commons Attribution (CC BY) license (<https://creativecommons.org/licenses/by/4.0/>).

1. Introduction

The Gleason score (GS) is an important determinant of the biological activity and aggressiveness of prostate cancer. The risk of prostate cancer progression is a determinant of its management. Prostate cancer is stratified into three risk categories that estimate the probability of disease progression. These categories are low risk (GS = 6 tumors), intermediate-risk (GS = 7 tumors), and high risk (GS \geq 8 tumors) [1,2]. Benign prostatic hyperplasia (BPH) can mimic prostate cancer symptoms. However, diagnosis would help rule cancer out in cases of BPH, which is due to a combination of stromal and glandular hyperplasia, predominantly of the transitional zone (TZ) [3]. Glandular tissue that is hyperintense on T₂-weighted (T₂W) images and stromal tissue that is hypointense can mimic prostate cancer [4,5]. Early differential diagnosis between prostate cancer and BPH is important because both the outcomes of and treatments for these two prostatic diseases are different.

Diffusion-weighted imaging (DWI) quantifies random Brownian motion properties of water molecules in tissues and cells. Restrictions on water diffusion in tissue and cells is inversely correlated to tissue cellularity and cell membrane integrity [6]. Diffusion of

molecules occurs across tissues from areas of restricted diffusion to areas with free diffusion. Apparent diffusion coefficient (ADC) is the net displacement of molecules across an area of tissue per second (mm^2/s). DWI and ADC maps obtained with magnetic resonance imaging (MRI) provide information regarding cellularity and grades of various tumors [7–9]. DWI is also used for tumor localization within the prostate [10–12]. In addition, ADC measurements derived from DWI are inversely correlated with GS [13–15]. The mean ADC is a commonly used ADC measurement because of its relative simplicity [16]. However, some studies have used other parameters, such as median ADC [17], or the 10th [18] or 25th [19] percentile values of the ADC histogram. It is important to clarify which of the ADC-derived parameters reflect tumor aggressiveness and can help distinguish between BPH and prostate cancer.

The present study aimed to assess the associations between prostate cancer aggressiveness as evaluated by GS and histogram-derived ADC parameters. We also aimed to determine which histogram ADC parameters may help distinguish between stromal hyperplasia (SH), glandular hyperplasia (GH), and low-grade, intermediate-grade, and high-grade prostate cancer lesions.

2. Materials and Methods

2.1. Patients

The local ethics committee approved the use of the clinical data for research and waived the requirement for written informed consent from the patients. Fifty-eight patients who had undergone 12-core and target biopsy of prostate (70 lesions) within 3 months after MRI study were included in this retrospective study; their characteristics are listed in Table 1. After prostatectomy, the prostatic specimens were submitted for histological investigation. The pathologists at our institution outlined each lesion on the microscopic slices and assigned a Gleason score. Thirty-nine lesions were prostate cancers (GS 6 = 7 lesions, GS 7 = 19 lesions, GS 8 = 11 lesions, GS 9 = 2 lesions), and thirty-one lesions were BPH (SH = 15 lesions, GH = 16 lesions).

Table 1. Summary of clinical and pathologic characteristics. For clinical characteristics, data are means and standard deviations with ranges in parentheses. For pathologic characteristics, data are numbers of patients with percentages in parentheses. For Gleason grade, data are numbers of tumor foci, with percentages in parentheses.

Variable	Value
Clinical characteristics	
Age (year)	69.3 ± 6.5 (51–84)
PSA (ng/mL)	17.5 ± 25.7 (4.2–196.0)
Pathologic characteristics	
pT2a	22 (56.4%)
pT2b	1 (2.5%)
pT2c	7 (17.9%)
pT3a	8 (20.5%)
pT4	1 (2.5%)
Gleason grade	
GS 3 + 3	7 (17.9%)
GS 3 + 4	17 (43.6%)
GS 4 + 3	2 (5.1%)
GS ≥ 8	13 (33.3%)

2.2. Magnetic Resonance Imaging

All MRI data were obtained using a 3.0 T MR scanner (Discovery MR750, GE Healthcare, Milwaukee, WI, USA) with a 32-channel body array coil with eight anterior and eight posterior elements. The sequences included fast spin echo (FSE) T₂W imaging and DWI. FSE T₂W imaging was performed with the following parameters: repetition

time (TR)/echo time (TE) = 8000/80 ms; matrix = 512×384 ; field of view (FOV) = 24 cm; section thickness = 4 mm with 0.4-mm intersection gap, 25 sections; number of excitations (NEX) = 2; array spatial sensitivity encoding technique (ASSET, GE Healthcare) factor = 1.5 and bandwidth = ± 41.7 kHz. DWI was performed with the following parameters: TR/TE = 7500/56.5 ms; matrix = 128×128 ; FOV = 30 cm; section thickness = 4 mm with 1.0-mm intersection gap, 26 sections; NEX = 5; bandwidth = ± 250 kHz; b-values = 0 and 1000 s/mm^2 ; ASSET factor = 2. The ADC maps were reconstructed at a GE workstation. While establishing the size and region for the region of interest (ROI), positioning in the larger area was considered in order to minimize the effect of region on the hemodynamic inhomogeneity of the tumor using T₂W images and ADC maps. The six histogram-derived ADC parameters (mean ADC, median ADC, minimum ADC, maximum ADC, 10th percentile ADC, and 25th percentile ADC) were calculated by applying these ROIs using IBM SPSS Statistics (Figure 1, Version 23, IBM, Armonk, NY, USA).

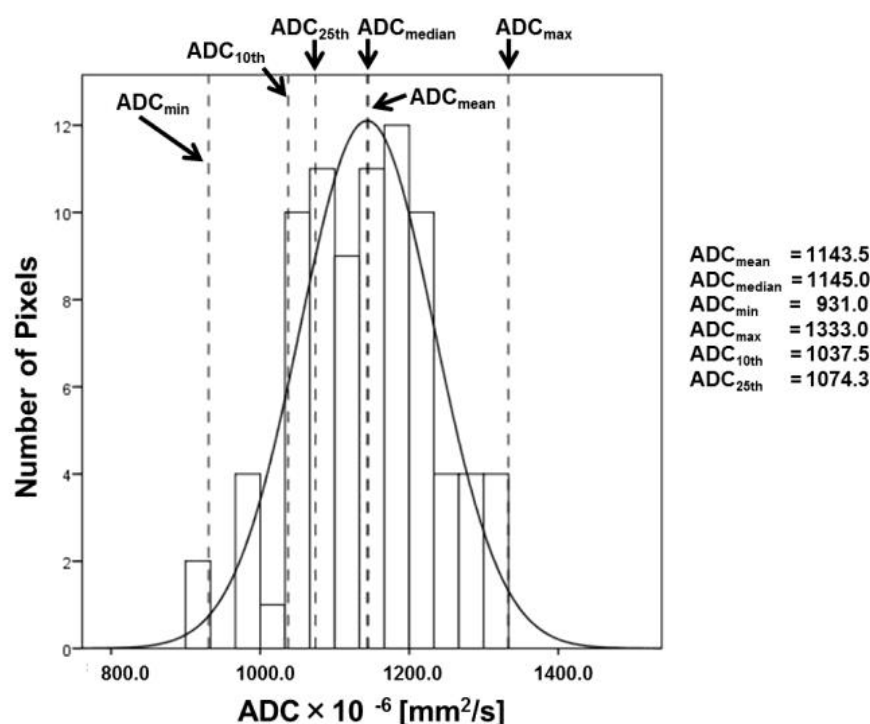


Figure 1. Typical histogram analysis of prostate cancer (Gleason score = 7) using the six histogram-derived ADC parameters. The mean ($1143.5 \times 10^{-6} \text{ mm}^2/\text{s}$), median ($1145.0 \times 10^{-6} \text{ mm}^2/\text{s}$), minimum ($931.0 \times 10^{-6} \text{ mm}^2/\text{s}$), maximum ($1333.1 \times 10^{-6} \text{ mm}^2/\text{s}$), and 10th ($1037.5 \times 10^{-6} \text{ mm}^2/\text{s}$) and 25th ($1074.3 \times 10^{-6} \text{ mm}^2/\text{s}$) percentile ADC values were determined from the ADC histogram.

2.3. Data Analysis

All of the values in all of the groups are expressed as means \pm standard deviations (SDs). All analyses were performed using Prism 5 (Version 5, GraphPad Software, Folsom, CA, USA). We used Tukey's tests for post-hoc analysis following the ANOVAs used to compare the six histogram-derived ADC parameters. Box plots of these ADC parameters were plotted for all lesions. The relationships between the ADC parameters and GS were analyzed in three subgroups (GS 6, GS 7, and GS ≥ 8). We performed nonparametric ROC curve analysis. The area under the ROC curve (AUC) was estimated to evaluate the ability of each ADC parameter to help discriminate tumor aggressiveness (GS 6 vs. GS 7 vs. GS ≥ 8). The ADC parameter with the highest AUC was identified. Spearman correlation coefficients were calculated to establish the between-patient correlation in each group. A *p* value of <0.05 was considered significant.

3. Results

3.1. Patients

In total, 70 tumor foci from 58 patients with confirmed prostatectomy were histologically detected. Of these lesions, 20 originated in the peripheral zone (PZ), 46 originated in the TZ, and the remaining 4 lesions covered both the PZ and the TZ. The clinical characteristics of the patients and those of the tumor foci ROIs are summarized in Table 1.

3.2. ADC Parameters of All Lesions

Figure 2 shows typical T₂W images (Figure 2A,D), ADC maps (Figure 2B,E), and ADC-derived histograms (Figure 2C,F) of BPH lesions. SH lesions are hypointense (Figure 2A) and GH lesions are hyperintense on T₂W images (Figure 2D). The ADC parameters of SH foci suggest restricted diffusion in the ADC map (Figure 2B, ADC_{mean} = 1171.6 × 10⁻⁶ mm²/s). However, the ADC values of GH foci are seen as bright regions on the ADC map (Figure 2E, ADC_{mean} = 1739.7 × 10⁻⁶ mm²/s).

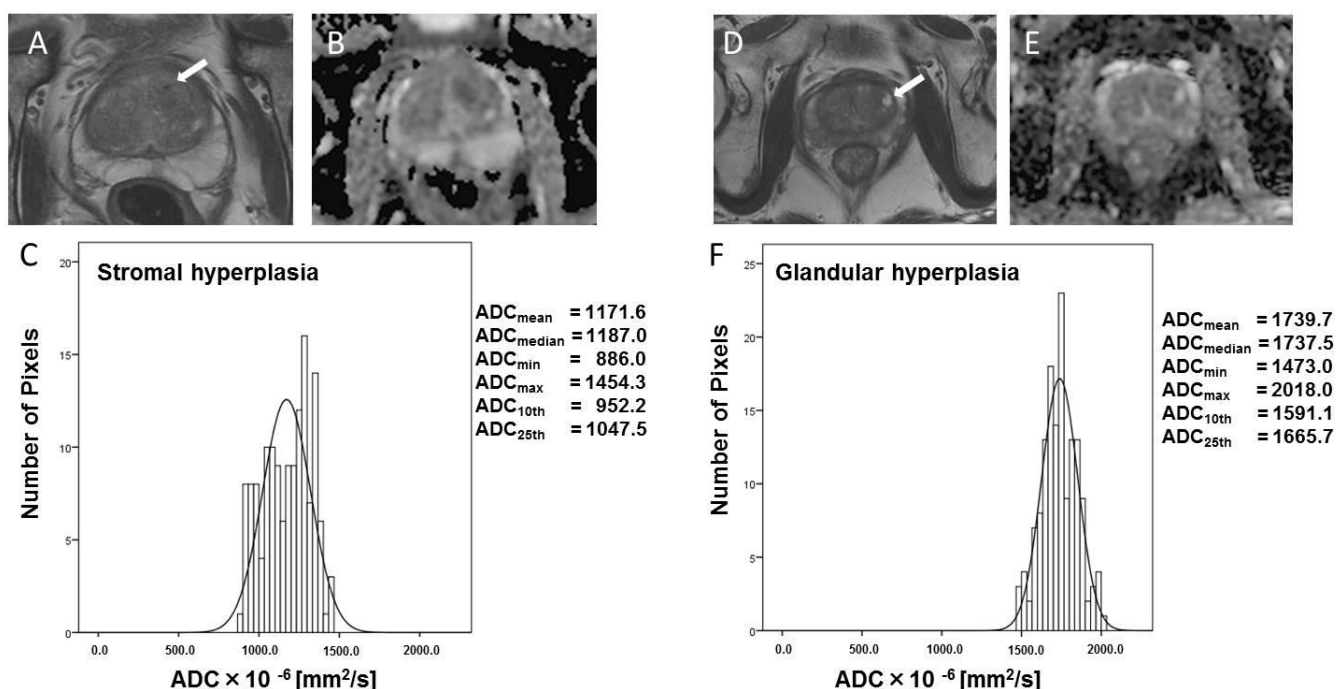


Figure 2. Typical histogram of BPH, and T₂W and ADC images (stromal hyperplasia and glandular hyperplasia). Typical T₂W images (A,D), ADC images (B,E), and ADC-derived histograms (C,F) for BPH. The ADC values of the SH foci reflect restricted diffusion in the ADC map ((B), ADC_{mean} = 1171.6 × 10⁻⁶ mm²/s). In contrast, the ADC values of the GH foci are seen as bright regions on the ADC map ((E), ADC_{mean} = 1739.7 × 10⁻⁶ mm²/s) and do not reflect restricted diffusion. The six histogram-derived ADC parameters are shown for each type of BPH. White arrows indicated BPH.

Typical T₂W images, ADC maps, and ADC-derived histograms from prostate cancer lesions as shown in Figure 3 (GS 6 and 7) and Figure 4 (GS 8 and 9). Prostate cancer lesions have low signal intensity on T₂W images (Figures 3A,D and 4A,D). The ADC values of GS 6 lesions reflect slightly restricted diffusion in the ADC map (Figure 3B, ADC_{mean} = 1256.4 × 10⁻⁶ mm²/s). However, the ADC values of GS 7 lesions are lower than that of GS 6 lesions on the ADC map (Figure 3E, ADC_{mean} = 1193.6 × 10⁻⁶ mm²/s). The ADC values of GS 8 (Figure 4B, ADC_{mean} = 773.5 × 10⁻⁶ mm²/s) and GS 9 (Figure 4D, ADC_{mean} = 647.2 × 10⁻⁶ mm²/s) lesions reflect restricted diffusion on ADC maps.

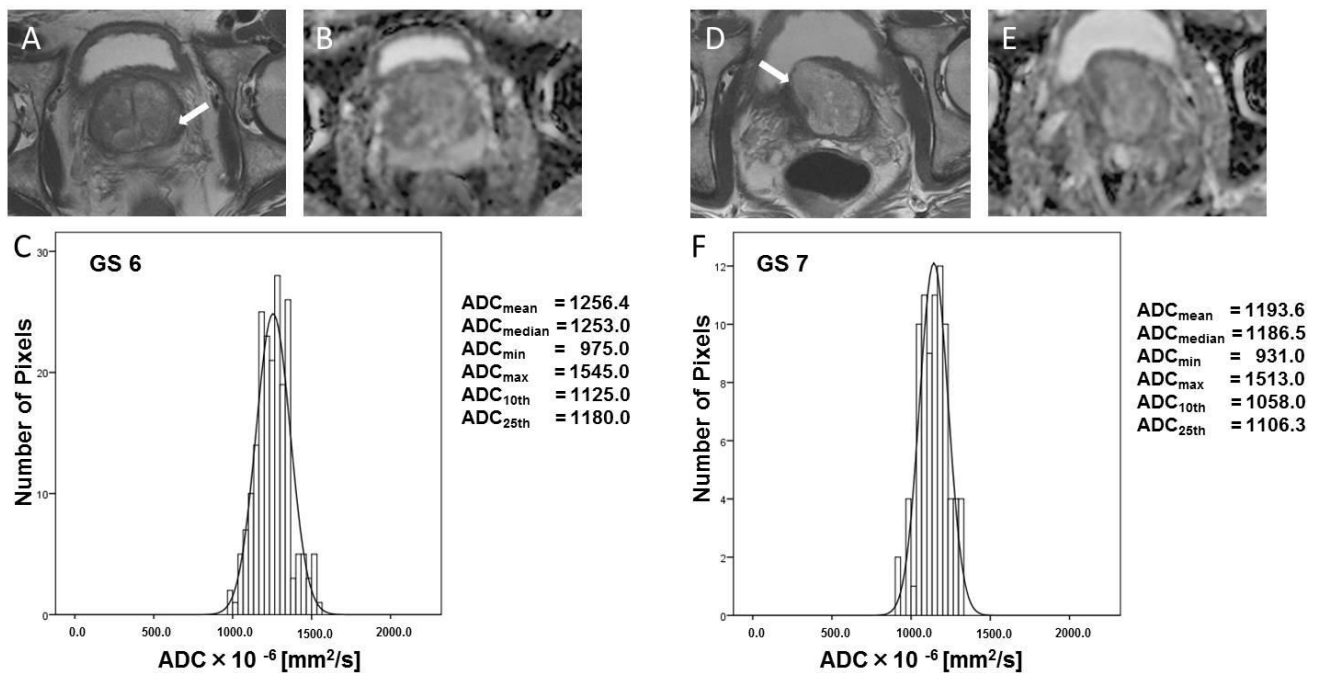


Figure 3. Typical histogram of tumor focus, and T₂W and ADC images (GS 6 and GS 7). GS = Gleason score. Typical T₂W images (A,D), ADC images (B,E), and ADC-derived histograms (C,F) for GS 6 and GS 7 prostate cancers. These T₂W images of prostate cancer illustrate the low signal intensity. The ADC values of the GS 6 lesion reflect slightly restricted diffusion on the ADC map ((B), ADC_{mean} = 1256.4 × 10⁻⁶ mm²/s). The ADC values of the GS 7 lesion are lower than that of the GS 6 lesion on the ADC map ((E), ADC_{mean} = 1193.6 × 10⁻⁶ mm²/s). White arrows indicated tumor foci.

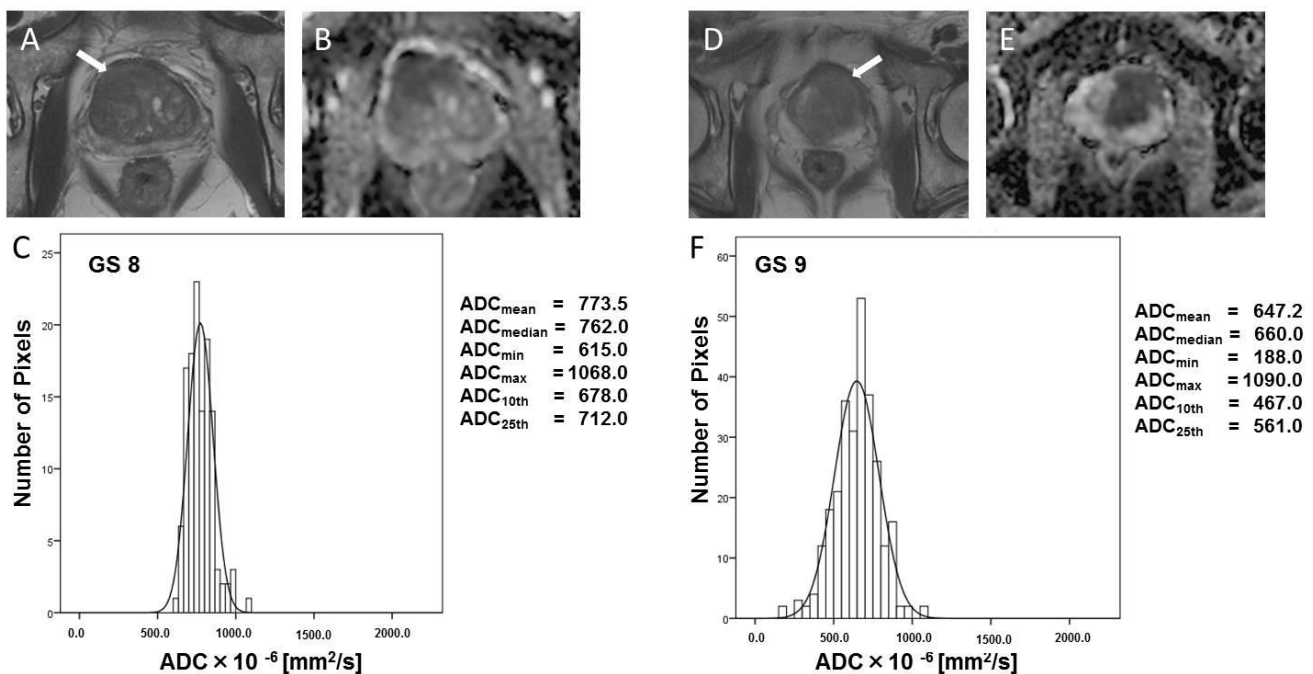


Figure 4. Typical histogram of tumor focus, and T₂W and ADC images (GS 8 and GS 9). GS = Gleason score. Typical T₂W images (A,D), ADC images (B,E), and ADC-derived histogram (C,F) for GS 8 and GS 9 prostate cancers. These T₂W images of prostate cancer illustrate the low signal intensity. The ADC values of the GS 8 ((B), ADC_{mean} = 773.5 × 10⁻⁶ mm²/s) and GS 9 ((D), ADC_{mean} = 647.2 × 10⁻⁶ mm²/s) lesions reflect restricted diffusion on the ADC map. White arrows indicated tumor foci.

Figure 5 shows box plots of the six histogram-derived ADC for the two BPH and three GS prostate cancer groups. All six ADC parameters differed significantly between SH and GH lesions (Figure 5, *** $p < 0.001$) and SH lesions and $GS \geq 8$ tumors (Figure 5, *** $p < 0.001$). All six ADC parameters differed significantly between GH lesions and the three GS prostate cancer groups (Figure 5, \$\$\$ $p < 0.001$). The 10th percentile ADC (Figure 5E, # $p < 0.05$) and 25th percentile ADC (Figure 5F, # $p < 0.05$) were significantly decreased in GS 7 lesions compared to GS 6 lesions. However, four other parameters (mean ADC, median ADC, minimum ADC, and maximum ADC) were not significantly different between GS 7 lesions and GS 6 lesions. All six ADC parameters differed significantly between the GS 6 and $GS \geq 8$ prostate cancer groups (Figure 5, ### $p < 0.001$). In addition, all six ADC parameters differed significantly between GS 7 and $GS \geq 8$ tumors (Figure 5, &&& $p < 0.001$). There were no significant differences in histogram-derived ADC parameters between SH and GS 6 lesions, and between the SH and GS 7 lesions.

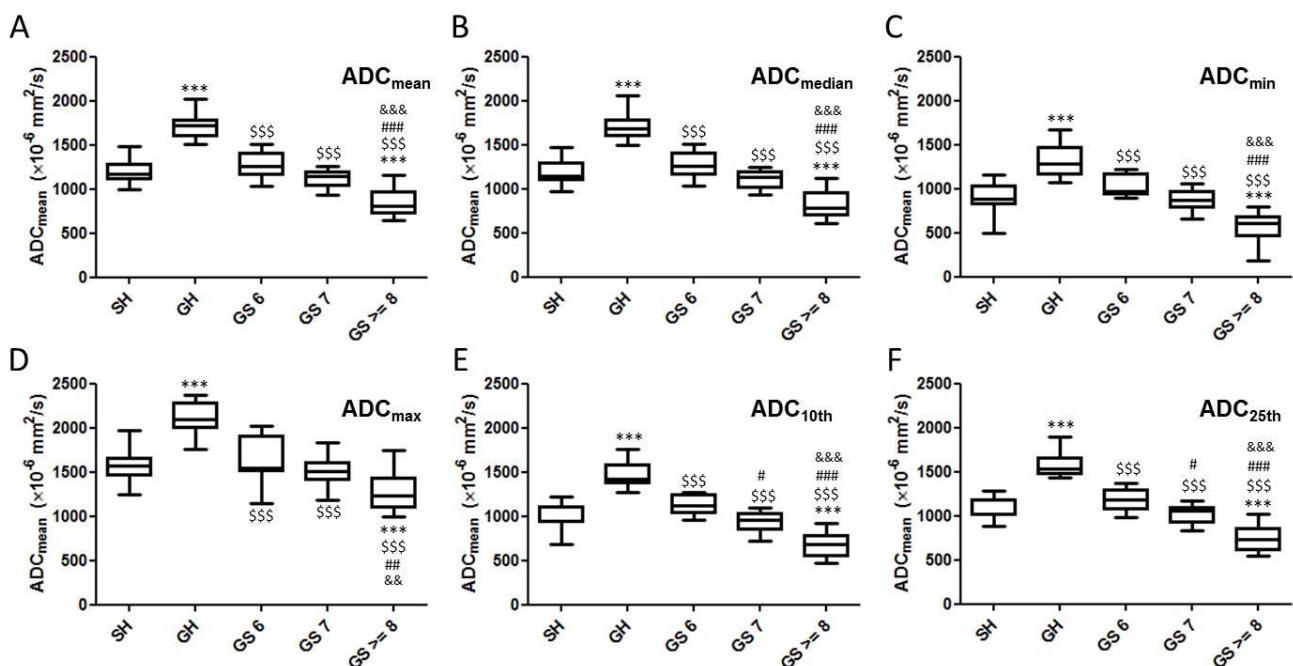


Figure 5. Box plots comparing the six histogram-derived ADC parameters in two BPH groups and the Gleason-graded groups. (A) ADC_{mean} ; (B) ADC_{median} ; (C) ADC_{min} ; (D) ADC_{max} ; (E) ADC_{10th} ; (F) ADC_{25th} . *: vs. SH (***: $p < 0.001$), \$: vs. GH (\$\$\$: $p < 0.001$), #: vs. GS 6 (#: $p < 0.05$, ##: $p < 0.01$, ###: $p < 0.001$), &: vs. GS7 (&&: $p < 0.01$, &&&: $p < 0.001$).

3.3. Ability of ADC Parameters to Help Differentiate among Tumors with Different GS

When differentiating between SH and GH lesions, mean, median, 10th percentile, and 25th percentile ADC values yielded the highest AUCs (1.00, $p < 0.0001$, Table 2), while minimum and maximum ADC values yielded the lowest AUCs (0.98, $p < 0.0001$, Table 2). When comparing SH lesions to GS 6 lesions, the AUC of the 10th percentile ADC value (0.82, $p = 0.02$, Table 2) was higher than that of the other parameters. When comparing SH lesions to GS 7 lesions, the AUCs of the six ADC parameters were not significantly different. When comparing the GH group to the three GS prostate cancer groups, the AUCs of the six ADC parameters were high (Table 3). When differentiating tumor foci with GS 6 from those with GS 7, the 10th percentile ADC yielded the highest AUC (0.87, $p < 0.001$, Table 4), while the maximum ADC yielded the lowest AUC (0.67, $p = 0.20$, Table 4). However, the AUC of the 10th percentile ADC was significantly higher than that of the mean ADC.

Table 2. Comparison of AUC values for used to differentiate tumor foci from stromal hyperplasia.

	SH vs. GS 6	<i>p</i> Value	SH vs. GS 7	<i>p</i> Value	SH vs. GS 8	<i>p</i> Value	SH vs. GH	<i>p</i> Value
Mean	0.70	0.15	0.62	0.27	0.97	<0.0001	1.00	<0.0001
Median	0.69	0.17	0.63	0.24	0.98	<0.0001	1.00	<0.0001
Minimum	0.76	0.05	0.59	0.41	0.96	<0.0001	0.98	<0.0001
Maximum	0.50	0.97	0.66	0.13	0.88	0.0003	0.98	<0.0001
10th	0.82	0.02	0.56	0.54	0.97	<0.0001	1.00	<0.0001
25th	0.73	0.08	0.59	0.41	0.97	<0.0001	1.00	<0.0001

Table 3. Comparison of AUC values used to differentiating tumor foci from glandular hyperplasia.

	GH vs. GS 6	<i>p</i> Value	GH vs. GS 7	<i>p</i> Value	GH vs. GS 8	<i>p</i> Value
Mean	1.00	<0.0001	1.0	<0.0001	1.0	<0.0001
Median	0.99	0.0002	1.0	<0.0001	1.0	<0.0001
Minimum	0.91	0.002	1.0	<0.0001	1.0	<0.0001
Maximum	0.94	0.001	1.0	<0.0001	1.0	<0.0001
10th	1.00	0.0002	1.0	<0.0001	1.0	<0.0001
25th	1.00	0.0002	1.0	<0.0001	1.0	<0.0001

Table 4. Comparison of AUC values used to differentiate tumor foci from prostate cancer.

	GS 6 vs. GS 7	<i>p</i> Value	GS 6 vs. GS 8	<i>p</i> Value	GS 7 vs. GS 8	<i>p</i> Value
Mean	0.78	0.04	0.98	0.0003	0.94	<0.0001
Median	0.79	0.03	0.99	0.0002	0.95	<0.0001
Minimum	0.79	0.03	1.00	0.0002	0.95	<0.0001
Maximum	0.67	0.20	0.86	0.008	0.83	0.002
10th	0.87	0.01	1.00	0.0002	0.94	<0.0001
25th	0.79	0.03	0.99	0.0002	0.95	<0.0001

3.4. Between-Subject Spearman Correlation Coefficients for Correlation of ADC Parameters with Gleason Score

Of the six ADC parameters, 10th percentile ADC correlated most strongly with GS ($r = -0.84, p < 0.001$), followed by the 25th percentile ADC ($r = -0.82, p < 0.001$), minimum ADC ($r = -0.83, p < 0.001$), median ADC ($r = -0.82, p < 0.001$), and mean ADC ($r = -0.80, p < 0.001$) (Table 5). Maximum ADC correlated most weakly with GS ($r = -0.59, p < 0.001$). These results indicate that the ADC-derived parameters inversely correlate with GS.

Table 5. Between-subjects Spearman correlation coefficients for correlations between ADC parameters and Gleason score.

	Spearman <i>r</i>	<i>p</i> Value
Mean	−0.80	<0.0001
Median	−0.82	<0.0001
Minimum	−0.83	<0.0001
Maximum	−0.59	<0.0001
10th	−0.84	<0.0001
25th	−0.82	<0.0001

4. Discussion

We found that the 10th and 25th percentile ADC parameters correlated best with the GS of prostate cancer lesions. In addition, the 10th and 25th percentile ADC parameters performed significantly better than the mean, median, minimum, and maximum ADC parameters in differentiating tumor foci with GS 6 from those with GS 7. The other four parameters (mean, median, minimum, and maximum ADCs) were not significantly different when comparing GS 6 lesions to GS 7 lesions. Thus, the 10th and 25th percentile ADCs were significantly better than the mean, median, minimum, and maximum ADCs when differentiating these two groups. There were no significant differences in ADC parameters between SH and GS 6 lesions, and SH and GS 7 lesions. These data indicate that the major challenge with ADC mapping is to differentiate SH lesions from those due to prostate cancer.

It has been suggested that enlargement of the TZ due to BPH associated with aging can lead to effacement of the central zone and thus poor differentiation between these two zones on MRI. GHs are easily differentiated from prostate cancer in the central gland owing to their predominantly hyperintense T₂ signal. However, a SH predominantly has hypointense T₂W characteristics similar to those of prostate cancer in the central gland. SH is significantly more cellular and denser and has less extracellular fluid than GH. These differences may explain the smaller ADCs observed for SH lesions [20]. Our results also indicate that it is not difficult to differentiate between GH and SH, or between GH and prostate cancer, using all six histogram-derived ADC parameters. Recognition of the different histologic subtypes of BPH is important in improving the diagnosis of prostate cancer. The range of Spearman correlation coefficients describing the relationships between ADC parameters and GS lesions in our study ($r = -0.59$ to -0.84) has a better range than those of previously reported associations between ADC parameters and GS [18,21]. Some overlap was observed between the ADC parameters of prostate cancer lesions of lower GS (GS 6 and GS 7) and those of SH lesions. A previous report shows that there are overlaps between mean ADCs of SH lesions and those of prostate cancer lesions [22]. These findings indicate that a major challenge in ADC mapping is the differentiation between hypointense SH lesions and prostate cancer lesions.

Conventional MRI is generally considered inadequate for evaluating prostate cancer because of the heterogeneous T₂ signal intensity in the normal TZ. Consequently, DWI is now incorporated into various cancer detection methods as an imaging biomarker [23]. Although the low ADC values found in most tumors have been attributed to increased cellular density, diffusion can also be influenced by tissue fibrosis, glandular and stromal structures, and tumor shape [24]. The predominant contribution to the DWI signal in the prostate is from extracellular components, such as tubular structures and their fluid content. There is also a lesser contribution from the extracellular stromal space and intracellular components, such as epithelial and stromal cells. In the PZ of the prostate, the abundant self-diffusion of water molecules within the predominant tubular components provide a high signal on ADC maps [25]. In our study, the 10th percentile ADC and 25th percentile ADC were significantly decreased in GS 7 lesions compared to GS 6 lesions. The 10th and 25th percentile ADC values outperform mean, median, minimum, and maximum ADC values when used to differentiate tumors with GS 6 from GS 7 tumors. In addition, the AUC of the 10th percentile ADC was significantly higher than that of the mean ADC in GS 7 lesions compared to GS 6 lesions. The 10th and 25th percentile ADC values outperform mean, median, minimum, and maximum ADC values when used to differentiate tumors with GS 6 from GS 7 tumors. This may be explained by the heterogeneous histological characteristics of prostate cancer foci. A previous report indicates that a large proportion of interspersed normal glandular prostatic tissue may influence mean ADC and median ADC values more than the 10th percentile ADC and 25th percentile ADC, thereby increasing the values of the former parameters [26]. In tumors densely packed with malignant cells, such as GS 8 and GS 9 tumors, the resulting ADC histogram may be less skewed and spread out. Therefore, differences between the evaluated ADC parameters may be less pronounced in

these cases. Focal areas of high cellularity are represented to a greater extent by the 10th and 25th percentile ADCs than by the mean, median, minimum, and maximum ADCs within tumors with heterogeneous cellularity, such as those with GS 6 and GS 7. Thus, dispersion of ADC values in low-grade GS 6 and intermediate-grade GS 7 tumors greatly affects the histogram-derived ADC parameters owing to the relatively low population of cancer cells in the ROI analysis.

Our study had several limitations. When comparing the mean ADC to the 10th percentile ADC, the 10th percentile ADC yielded a higher AUC when differentiating prostate cancer from healthy prostatic tissue. However, the two parameters yielded the same AUC when differentiating tumor foci with GS 6 from those with GS 7 in a previous report [18]. This discrepancy between the findings of the previous study and those of our study may be related to the selection of the b-values in the DWI used for ADC determination. Two different sets of b-values were used to acquire diffusion-weighted MR images in the previous study [18], while we used the same b-values in all patients. The conditions of the MR sequences are important when evaluating ADC values in prostate cancer. It is thus important to select and set appropriate b-values. This study was a retrospective study with a relatively small sample size, which may have been influenced by selection and verification biases. Previous reports that Gleason score from needle biopsy can often differ from that determined with radical prostatectomy [27] and with immediate repeat biopsies [28]. The reliability of the correlation between MR imaging and the specimens is crucial. Although we tried to minimize inaccuracies by performing the correlation carefully and avoiding the inclusion of healthy tumor tissue in the ROIs, some uncertainty remains. In addition, we did not normalize the histograms to reduce the effects of tumor volumes. Finally, future studies should evaluate the reproducibility of the absolute ADC values in different vendors and field strengths, as well as the choice of b-values.

5. Conclusions

Our results suggest that the 10th and 25th percentile ADCs can be used to more accurately differentiate lesions with GS 6 from those with GS 7 than other ADC parameters, while our data indicate that the major challenge with ADC mapping is to differentiate between SH and GS 6, and SH and GS 7. These parameters can be used as a non-invasive biomarker to predict the Gleason score of the prostate cancer patients.

Author Contributions: Conceptualization, S.S., Y.K., J.U. and T.H.; methodology, S.S.; investigation, S.S.; data curation, S.S.; writing—original draft preparation, S.S.; writing—review and editing, S.S.; supervision, S.S.; funding acquisition, S.S. All authors have read and agreed to the published version of the manuscript.

Funding: This research was funded by the Japan Society for the Promotion of Science (JSPS) KAKENHI (grant number; T16K090170, 19K08172).

Institutional Review Board Statement: This study was approved by the Osaka University Clinical Research Review Committee (Permission number: 14278-2). All procedures performed in studies involving human participants were in accordance with the ethical standards of the institutional research committee and with the 1964 Helsinki declaration and its later amendments or comparable ethical standards.

Informed Consent Statement: The local ethics committee approved the use of the clinical data for research and waived the requirement for written informed consent from the patients.

Data Availability Statement: Not applicable.

Conflicts of Interest: The authors declare no conflict of interest.

References

1. Heidenreich, A.; Bastian, P.J.; Bellmunt, J.; Bolla, M.; Joniau, S.; van der Kwast, T.; Mason, M.; Matveev, V.; Wiegel, T.; Zattoni, F.; et al. EAU guidelines on prostate cancer. part 1: Screening, diagnosis, and local treatment with curative intent-update 2013. *Eur. Urol.* **2014**, *65*, 124–137. [[CrossRef](#)] [[PubMed](#)]
2. Mottet, N.; Bellmunt, J.; Bolla, M.; Briers, E.; Cumberbatch, M.G.; De Santis, M.; Fossati, N.; Gross, T.; Henry, A.M.; Joniau, S.; et al. EAU-ESTRO-SIOG Guidelines on Prostate Cancer. Part 1: Screening, Diagnosis, and Local Treatment with Curative Intent. *Eur. Urol.* **2016**. [[CrossRef](#)] [[PubMed](#)]
3. Choi, J.D.; Kim, J.H.; Ahn, S.H. Transitional Zone Index as a Predictor of the Efficacy of alpha-Blocker and 5alpha-Reductase Inhibitor Combination Therapy in Korean Patients with Benign Prostatic Hyperplasia. *Urol. Int.* **2016**, *96*, 406–412. [[CrossRef](#)] [[PubMed](#)]
4. Schiebler, M.L.; Tomaszewski, J.E.; Bezzi, M.; Pollack, H.M.; Kressel, H.Y.; Cohen, E.K.; Altman, H.G.; Geftter, W.B.; Wein, A.J.; Axel, L. Prostatic carcinoma and benign prostatic hyperplasia: Correlation of high-resolution MR and histopathologic findings. *Radiology* **1989**, *172*, 131–137. [[CrossRef](#)]
5. Ishida, J.; Sugimura, K.; Okizuka, H.; Kaji, Y.; Moriyama, M.; Nagaoka, S.; Mizutani, M.; Ishida, T. Benign prostatic hyperplasia: Value of MR imaging for determining histologic type. *Radiology* **1994**, *190*, 329–331. [[CrossRef](#)]
6. Uhl, M.; Althoefer, C.; Kontrny, U.; Il'yasov, K.; Buchert, M.; Langer, M. MRI-diffusion imaging of neuroblastomas: First results and correlation to histology. *Eur. Radiol.* **2002**, *12*, 2335–2338. [[CrossRef](#)]
7. Squillaci, E.; Manenti, G.; Cova, M.; Di Roma, M.; Miano, R.; Palmieri, G.; Simonetti, G. Correlation of diffusion-weighted MR imaging with cellularity of renal tumours. *Anticancer Res.* **2004**, *24*, 4175–4179.
8. Yamasaki, F.; Kurisu, K.; Satoh, K.; Arita, K.; Sugiyama, K.; Ohtaki, M.; Takaba, J.; Tominaga, A.; Hanaya, R.; Yoshioka, H.; et al. Apparent diffusion coefficient of human brain tumors at MR imaging. *Radiology* **2005**, *235*, 985–991. [[CrossRef](#)]
9. Kishimoto, K.; Tajima, S.; Maeda, I.; Takagi, M.; Ueno, T.; Suzuki, N.; Nakajima, Y. Endometrial cancer: Correlation of apparent diffusion coefficient (ADC) with tumor cellularity and tumor grade. *Acta Radiol.* **2016**, *57*, 1021–1028. [[CrossRef](#)]
10. Kim, C.K.; Park, B.K.; Lee, H.M.; Kwon, G.Y. Value of diffusion-weighted imaging for the prediction of prostate cancer location at 3T using a phased-array coil: Preliminary results. *Investig. Radiol.* **2007**, *42*, 842–847. [[CrossRef](#)]
11. Chen, M.; Dang, H.D.; Wang, J.Y.; Zhou, C.; Li, S.Y.; Wang, W.C.; Zhao, W.F.; Yang, Z.H.; Zhong, C.Y.; Li, G.Z. Prostate cancer detection: Comparison of T2-weighted imaging, diffusion-weighted imaging, proton magnetic resonance spectroscopic imaging, and the three techniques combined. *Acta Radiol.* **2008**, *49*, 602–610. [[CrossRef](#)] [[PubMed](#)]
12. Yagci, A.B.; Ozari, N.; Aybek, Z.; Duzcan, E. The value of diffusion-weighted MRI for prostate cancer detection and localization. *Diagn. Interv. Radiol.* **2011**, *17*, 130–134. [[CrossRef](#)] [[PubMed](#)]
13. Hegde, J.V.; Mulkern, R.V.; Panych, L.P.; Fennessy, F.M.; Fedorov, A.; Maier, S.E.; Tempany, C.M. Multiparametric MRI of prostate cancer: An update on state-of-the-art techniques and their performance in detecting and localizing prostate cancer. *J. Magn. Reson. Imaging* **2013**, *37*, 1035–1054. [[CrossRef](#)] [[PubMed](#)]
14. Barentsz, J.O.; Richenberg, J.; Clements, R.; Choyke, P.; Verma, S.; Villeirs, G.; Rouviere, O.; Logager, V.; Futterer, J.J. ESUR prostate MR guidelines 2012. *Eur. Radiol.* **2012**, *22*, 746–757. [[CrossRef](#)] [[PubMed](#)]
15. Rosenkrantz, A.B.; Triolo, M.J.; Melamed, J.; Rusinek, H.; Taneja, S.S.; Deng, F.M. Whole-lesion apparent diffusion coefficient metrics as a marker of percentage Gleason 4 component within Gleason 7 prostate cancer at radical prostatectomy. *J. Magn. Reson. Imaging* **2015**, *41*, 708–714. [[CrossRef](#)] [[PubMed](#)]
16. Quon, J.; Kielar, A.Z.; Jain, R.; Schieda, N. Assessing the utilization of functional imaging in multiparametric prostate MRI in routine clinical practice. *Clin. Radiol.* **2015**, *70*, 373–378. [[CrossRef](#)]
17. Hambrock, T.; Somford, D.M.; Huisman, H.J.; van Oort, I.M.; Witjes, J.A.; Hulsbergen-van de Kaa, C.A.; Scheenen, T.; Barentsz, J.O. Relationship between apparent diffusion coefficients at 3.0-T MR imaging and Gleason grade in peripheral zone prostate cancer. *Radiology* **2011**, *259*, 453–461. [[CrossRef](#)]
18. Peng, Y.; Jiang, Y.; Yang, C.; Brown, J.B.; Antic, T.; Sethi, I.; Schmid-Tannwald, C.; Giger, M.L.; Eggen, S.E.; Oto, A. Quantitative analysis of multiparametric prostate MR images: Differentiation between prostate cancer and normal tissue and correlation with Gleason score—A computer-aided diagnosis development study. *Radiology* **2013**, *267*, 787–796. [[CrossRef](#)]
19. Kobus, T.; Vos, P.C.; Hambrock, T.; De Rooij, M.; Hulsbergen-Van de Kaa, C.A.; Barentsz, J.O.; Heerschap, A.; Scheenen, T.W. Prostate cancer aggressiveness: In vivo assessment of MR spectroscopy and diffusion-weighted imaging at 3 T. *Radiology* **2012**, *265*, 457–467. [[CrossRef](#)]
20. Noworolski, S.M.; Vigneron, D.B.; Chen, A.P.; Kurhanewicz, J. Dynamic contrast-enhanced MRI and MR diffusion imaging to distinguish between glandular and stromal prostatic tissues. *Magn. Reson. Imaging* **2008**, *26*, 1071–1080. [[CrossRef](#)]
21. Oto, A.; Yang, C.; Kayhan, A.; Tretiakova, M.; Antic, T.; Schmid-Tannwald, C.; Eggen, S.; Karczmar, G.S.; Stadler, W.M. Diffusion-weighted and dynamic contrast-enhanced MRI of prostate cancer: Correlation of quantitative MR parameters with Gleason score and tumor angiogenesis. *AJR Am. J. Roentgenol.* **2011**, *197*, 1382–1390. [[CrossRef](#)] [[PubMed](#)]
22. Park, S.Y.; Kim, C.K.; Park, B.K.; Ha, S.Y.; Kwon, G.Y.; Kim, B. Diffusion-tensor MRI at 3 T: Differentiation of central gland prostate cancer from benign prostatic hyperplasia. *AJR Am. J. Roentgenol.* **2014**, *202*, W254–W262. [[CrossRef](#)] [[PubMed](#)]
23. Padhani, A.R.; Liu, G.; Koh, D.M.; Chenevert, T.L.; Thoeny, H.C.; Takahara, T.; Dzik-Jurasz, A.; Ross, B.D.; Van Cauteren, M.; Collins, D.; et al. Diffusion-weighted magnetic resonance imaging as a cancer biomarker: Consensus and recommendations. *Neoplasia* **2009**, *11*, 102–125. [[CrossRef](#)] [[PubMed](#)]

24. Chenevert, T.L.; Sundgren, P.C.; Ross, B.D. Diffusion imaging: Insight to cell status and cytoarchitecture. *Neuroimaging Clin. N. Am.* **2006**, *16*, 619–632. [[CrossRef](#)]
25. Tamada, T.; Sone, T.; Jo, Y.; Yamamoto, A.; Yamashita, T.; Egashira, N.; Imai, S.; Fukunaga, M. Prostate cancer: Relationships between postbiopsy hemorrhage and tumor detectability at MR diagnosis. *Radiology* **2008**, *248*, 531–539. [[CrossRef](#)] [[PubMed](#)]
26. Langer, D.L.; van der Kwast, T.H.; Evans, A.J.; Sun, L.; Yaffe, M.J.; Trachtenberg, J.; Haider, M.A. Intermixed normal tissue within prostate cancer: Effect on MR imaging measurements of apparent diffusion coefficient and T2-sparse versus dense cancers. *Radiology* **2008**, *249*, 900–908. [[CrossRef](#)]
27. King, C.R.; Long, J.P. Prostate biopsy grading errors: A sampling problem? *Int. J. Cancer* **2000**, *90*, 326–330. [[CrossRef](#)]
28. Berglund, R.K.; Masterson, T.A.; Vora, K.C.; Eggener, S.E.; Eastham, J.A.; Guillonneau, B.D. Pathological upgrading and up staging with immediate repeat biopsy in patients eligible for active surveillance. *J. Urol.* **2008**, *180*, 1964–1967; discussion 1967–1968. [[CrossRef](#)]